Quantum hologram of macroscopically entangled light via the mechanism of diffuse light storage

2012 J. Phys. B: At. Mol. Opt. Phys. 45 124012

(http://iopscience.iop.org/0953-4075/45/12/124012)

J. Phys. B: At. Mol. Opt. Phys. **45** (2012) 124012 (8pp) doi:10.1088/0953-4075/45/12/124012

Quantum hologram of macroscopically entangled light via the mechanism of diffuse light storage

L V Gerasimov[1], I M Sokolov[1], D V Kupriyanov[1] and M D Havey[2]

[1] Department of Theoretical Physics, St-Petersburg State Polytechnic University, 195251 St-Petersburg, Russia
[2] Department of Physics, Old Dominion University, Norfolk, VA 23529, USA

E-mail: kupr@dk11578.spb.edu

Received 18 January 2012, in final form 9 April 2012
Published 8 June 2012
Online at stacks.iop.org/JPhysB/45/124012

Abstract
In this paper, we consider a quantum memory scheme for light diffusely propagating through a spatially disordered atomic gas. A unique characteristic is enhanced trapping of the signal light pulse by quantum multiple scattering, which can be naturally integrated with the mechanism of stimulated Raman conversion into a long-lived spin coherence. Then, the quantum state of the light can be mapped onto the disordered atomic spin subsystem and can be stored in it for a relatively long time. The proposed memory scheme can be applicable for storage of the macroscopic analogue of the $\Psi^{(-)}$ Bell state and the prepared entangled atomic state performs its quantum hologram, which suggests the possibility of further quantum information processing.

(Some figures may appear in colour only in the online journal)

1. Introduction

Quantitative recognition of the important role played by disorder in studies of transport in condensed matter physics was stimulated by the seminal research of Anderson [1] more than 50 years ago. A key element of investigations is in understanding the transition of wave transport from diffusive to localized behaviour, Anderson localization. For three-dimensional systems, this occurs in the vicinity of the so-called Ioffe–Regel condition, $kl \sim 1$, where k is the local wave vector and l the mean free path [2]. Even when this condition is not satisfied, that is, in the *weak localization* regime, a constellation of physical effects can occur, including the appearance of universal conductance fluctuations, antilocalization in the presence of magnetic interactions and, in quasi one-dimensional systems, the development of universal descriptions of physical observables when these quantities are suitably normalized by their associated variances.

Recognition of weak localization and disorder-induced coherent effects in optical systems was first made by Wolf *et al* [3] and Albada *et al* [4] in 1985, when coherent backscattering of light from dilute disordered scattering samples was observed. The development of technologies to produce ultracold atom samples led to the observation and study of coherent multiple scattering, including coherent backscattering of resonance radiation, by Labeyrie *et al* [5, 6]. These results were confirmed by Kulatunga *et al* [7, 8]. There are important distinctions between coherent light propagation in ultracold atomic systems and in samples of classical scatterers. One of the most important of these is that in atomic systems the state of the scatterers themselves can be modified by the scattering process itself. Since these early measurements, and associated theoretical descriptions, the role of disorder in light scattering in ultracold gases has extended over a wide range, from light propagation in a nearly radiation trapping regime [9, 10], to high-density gases where dipole–dipole interactions are critical and where collective scattering dominates [11], and to novel cooperative scattering effects [12]. Theoretical predictions [13, 14] have also led to the observation of random lasing, evocatively described as a photon bomb [15]. Finally, we should point out recent beautiful experiments on one- [16, 17] and three-dimensional [18] localization of matter waves derived from a Bose–Einstein

condensate. Such studies promise incisive studies of the role of interactions and imposed quantum correlations on the Anderson transition from extended to localized waves.

Recent theoretical studies have also examined the role of disorder under conditions of electromagnetically induced transparency (EIT) or under the similar process of electromagnetically induced amplification (EIA) [19, 20]. These investigations have prompted initial examination of the possibility that coherent multiple scattering, mediated by a disordered assemblage of atoms, could lead to the development of a diffuse dark-state polariton. Such a quasi-particle would be analogous to the more familiar dark-state polariton, but would have the associated spin wave coherence distributed among a disordered collection of ultracold atoms. This, in turn, stimulated the possibility that the much longer scattering path lengths possible in disordered systems (in comparison with the path length associated with propagation of the coherent forward scattered beam in traditional EIT based systems) might lead to improvements of, or a different type of EIA-based quantum memory for light [20].

At present, atomic systems have shown themselves as promising candidates for effective light storage, see recent reviews of the problem in [21, 22]. For example, quite recently a very high-level efficiency of light storage in a dense gas of ^{87}Rb atoms, via the gradient echo protocol, has been reported in [23]. Among other studies, it has shown the promising capability of such an approach towards a practical atomic memory for quantum states of light. However, the problem of reliable light storage remains an area of active investigation and a variety of alternative approaches may be useful in different situations, and may lead to further improvement of atomic memory efficiencies and reliability in either cold or warm atomic vapours, see [24, 25].

One possible alternative approach implies special arrangements of effective light storage in a cold atomic sample in the diffusive regime, see [20]. In this case, in an optically dense atomic sample with a given number of atoms, the actual random optical path of light transport becomes much longer than for the single passage of the same sample in the forward direction either under conditions of the EIT effect or in the near resonance transparency spectral window. As a rough estimate, if for an atomic medium formed in a MOT the optical depth on a closed resonance transition is b_0, then the actual diffusive path can be $b_\Sigma \sim b_0^2$, i.e. b_0 times longer. For typical parameters $b_0 \sim 20$–50, we have a very promising enhancement resource for the light storage via stimulated Raman conversion of the signal pulse as it interacts with the atomic sample in the diffusive regime.

In this paper, we will discuss such a diffusive quantum memory mechanism in the context of its application to storage of macroscopically entangled light. One experimental technique for generation of polarization-entangled light by near subthreshold spontaneous parametric down conversion (SPDC) type-II light source is well established now, see [26]. An alternative approach under development utilizes the polarization self-rotation effect to generate significantly polarization-squeezed light [27–30]. The latter approach has the substantial advantage of generating quantum states of light

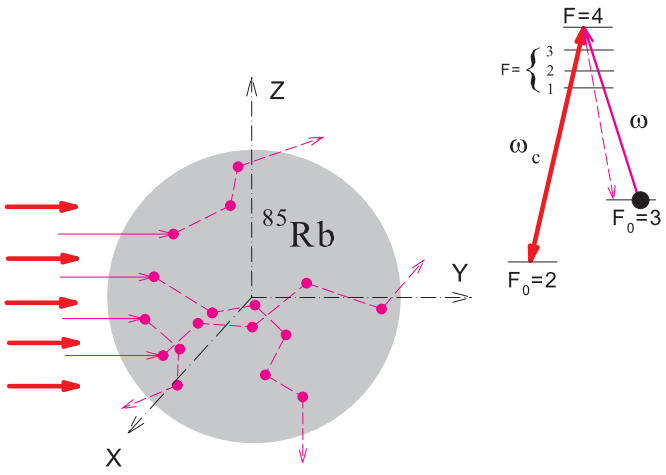

Figure 1. The mechanism of diffuse storage of light for the example of light trapping on the $F_0 = 3 \rightarrow F = 4$ closed transition in ^{85}Rb. The diffuse propagation of a signal mode of frequency ω is indicated by pink thin lines and arrows. The diffusion process is affected by a strong control mode of frequency ω_c indicated by red and thick arrows. This converts a signal pulse into a long-lived spin coherence in the atomic subsystem.

with very narrow bandwidth and tunability in the vicinity of atomic resonances, important characteristics for an atomic physics based quantum memory. In either case, the generated light possesses the quantum information encoded by the same mechanism and, in the particular case of [26], in the strongly correlated photon numbers related to different polarization modes. As we show here, each mode can be stored in a particular memory unit via transforming the unknown number of photons to the equally unknown number of atoms repopulating the signal level. Importantly, the specifics of the considered memory scheme and of the stored quantum state is that it is possible to investigate the quality of the storage of the quantum correlations in the standard interferometric technique via relevant operations with the prepared quantum hologram.

2. The mechanism of diffuse light storage

The considered light storage mechanism is based on stimulated Raman conversion of a signal pulse into a long-lived spin coherence. The main difference with traditional approaches, see [21, 22], requires that the pulse diffusely propagates through an atomic sample. The hyperfine energy structure of heavy alkali-metal atoms, such as rubidium or cesium, allows convenient integration of these processes [20]. In figure 1, we illustrate this through the example of the $F_0 = 3 \rightarrow F = 4$ closed transition in ^{85}Rb. The crucial point for the effects is the presence and strong action of the control laser mode repopulating the atoms from the background $F_0 = 3$ hyperfine sublevel to the signal $F_0 = 2$ sublevel via Raman interaction with the upper $F = 3, 2$ states. As a result, the quantum state of light can be mapped onto a disordered hyperfine coherence and collectivized by the atomic ensemble. Under ideal conditions, without relaxation and atomic losses, the stored state effectively performs a quantum hologram of the signal light, which can survive a relatively long time in the atomic spin subsystem.

To make such a memory scheme feasible, the following two important criteria should be fulfilled. In the Raman mechanism, only those pulses can be effectively delayed, which have relatively narrow spectral width

$$\Delta\omega_{\text{pulse}} \ll \Gamma_{\text{AT}} b_\Sigma \sim O(1)\,\frac{\overline{\Omega_c^2}}{\Delta^2}\gamma b_\Sigma. \qquad (1)$$

Here, $\Gamma_{\text{AT}} \sim O(1)\frac{\overline{\Omega_c^2}}{\Delta^2}\gamma$, where γ is the natural radiative decay rate, is an estimate for the bandwidth of the Autler–Townes (AT) resonance, created by the control field. The bandwidth is expressed by the averaged (indicated by overbar) Rabi frequency for the control field Ω_c and by its averaged detuning Δ from those upper state hyperfine sublevels, which are involved in the Raman process. In our case, Δ can be estimated by the hyperfine splitting Δ_{hpf} between the $F = 4$ and $F = 3$ sublevels in the upper state. The dimensionless optical depth b_Σ can be estimated as $b_\Sigma \sim n_0(\lambda/2\pi)^2 L_\Sigma$, where n_0 is a typical density of atoms in the sample, λ is the radiation wavelength and L_Σ is the length of a diffusive path of the signal pulse in the sample, see figure 1. Physically, condition (1) constrains the spectral domain where dispersion effects are manifestable. However, for the spectrally narrow pulses there can be a strong influence of the spontaneous Raman losses initiated by the scattering on the absorption part of the AT resonance. To guarantee that the spontaneous scattering is a negligible effect, the following inequality, as an alternative to (1), should be fulfilled

$$\Delta\omega_{\text{pulse}} \gg \Gamma_{\text{AT}}\sqrt{b_\Sigma} \sim O(1)\,\frac{\overline{\Omega_c^2}}{\Delta^2}\gamma\sqrt{b_\Sigma}. \qquad (2)$$

Considered together both inequalities (1) and (2) lead to an analogue of the well-known requirement for atomic memory units $b_\Sigma \gg 1$, see [21]; i.e. in our case the signal pulse should pass a long transport path in the medium. As we pointed out above, in the diffusive regime this path can be made very long.

The optimal pulse spectrum seems $\Delta\omega_{\text{pulse}} \lesssim \gamma$ which justifies the substantial trapping of light via the multiple scattering mechanism. In this case, the variation of the Rabi frequency of the control mode is bounded by the above inequalities, which together comprise the losses and dispersion effects. In reality, even a standard one-dimensional realization of the quantum memory protocol requires serious optimization efforts, see [21]. Apparently, in the discussed three-dimensional configuration, which is principally based on the D_2-line multilevel energy structure of alkali-metal atom, the optimization scheme is expected to be much more complicated. Inequalities (1) and (2) give us a physically clear but only rough approximation, which we can consider as only the simplest qualitative recommendation. In figure 2, a typical spectral dependence for the dielectric susceptibility of the atomic sample, modified by the presence of the control mode, is shown. The spectra are reproduced in the vicinity of the $F_0 = 3 \to F = 4$ resonance line of ^{85}Rb and Δ is the relevant frequency detuning. The sample susceptibility is scaled by the dimensionless density of atoms $n_0(\lambda/2\pi)^3$ and we address the reader to the appendix to follow the calculation details. The upper curve indicates the overall 'absorption' profile, which is actually responsible not for absorption but for incoherent light scattering, and the lower curves select the contribution of the absorption and dispersion parts of the AT resonance only. The initial polarization direction for the signal mode **e** and the polarization of the control mode $\mathbf{e}_c$ are related to the reference frame and the excitation geometry shown in figure 1. The spectrum of the signal pulse, shown by the pink filled area, is narrower than the original Lorentz profile of the non-disturbed atomic resonance $F_0 = 3 \to F = 4$ but essentially broader than the AT resonance. We consider the flat spectral profile to follow how the photons having a frequency uncertainty randomly distributed in the selected spectral area could be potentially delayed via the diffuse memory protocol.

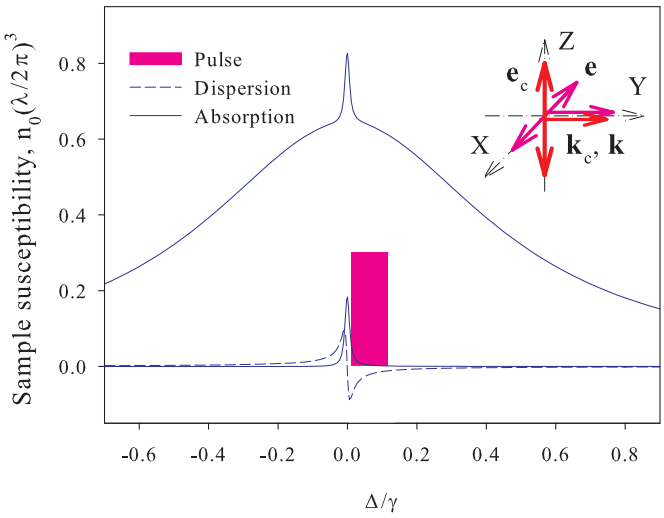

Figure 2. Dielectric susceptibility of the sample versus the pulse spectrum. The spectra are shown in the vicinity of the $F_0 = 3 \to F = 4$ resonance line of ^{85}Rb and Δ is the relevant frequency detuning. The susceptibility is scaled by the dimensionless density of atoms $n_0(\lambda/2\pi)^3$. The upper curve indicates the overall absorption profile modified by the presence of the control mode and the lower curves select the contribution of the absorption and dispersion parts of the AT resonance only. The initial polarization and propagation directions for the signal mode **e**, **k** as well as the polarization and propagation directions of the control mode $\mathbf{e}_c$, $\mathbf{k}_c$ are related to the reference frame and the excitation geometry shown in figure 1. The pulse spectrum is shown by the pink filled area.

In figure 3, we demonstrate a portion of our Monte Carlo simulations of the process, see the appendix. The performed calculations have been carried out for a spherical atomic cloud consisting of ^{85}Rb atoms with a Gaussian-type radial distribution characterized by a squared variance r_0^2. The optical depth for a light ray propagating through the central point of the cloud is given by $b_0 = \sqrt{2\pi}\, n_0\, \sigma_0\, r_0$, where n_0 is the peak density of atoms and σ_0 is the resonance cross-section for the $F_0 = 3 \to F = 4$ transition. In our calculations, we used $b_0 = 20$, which is an example of attainable depth in cold atom experiments with alkali-metal atom samples prepared in a MOT. The graphs of figure 3 subsequently show how the delay effect associated with the control field is accumulated as the scattering order is increased. In our numerical simulations, we assumed the simplest atomic distribution with equal population of all the Zeeman sublevels in the background state ($F_0 = 3$). This creates the AT resonance with rather small amplitude, see figure 2. The resonance could be essentially enhanced for the

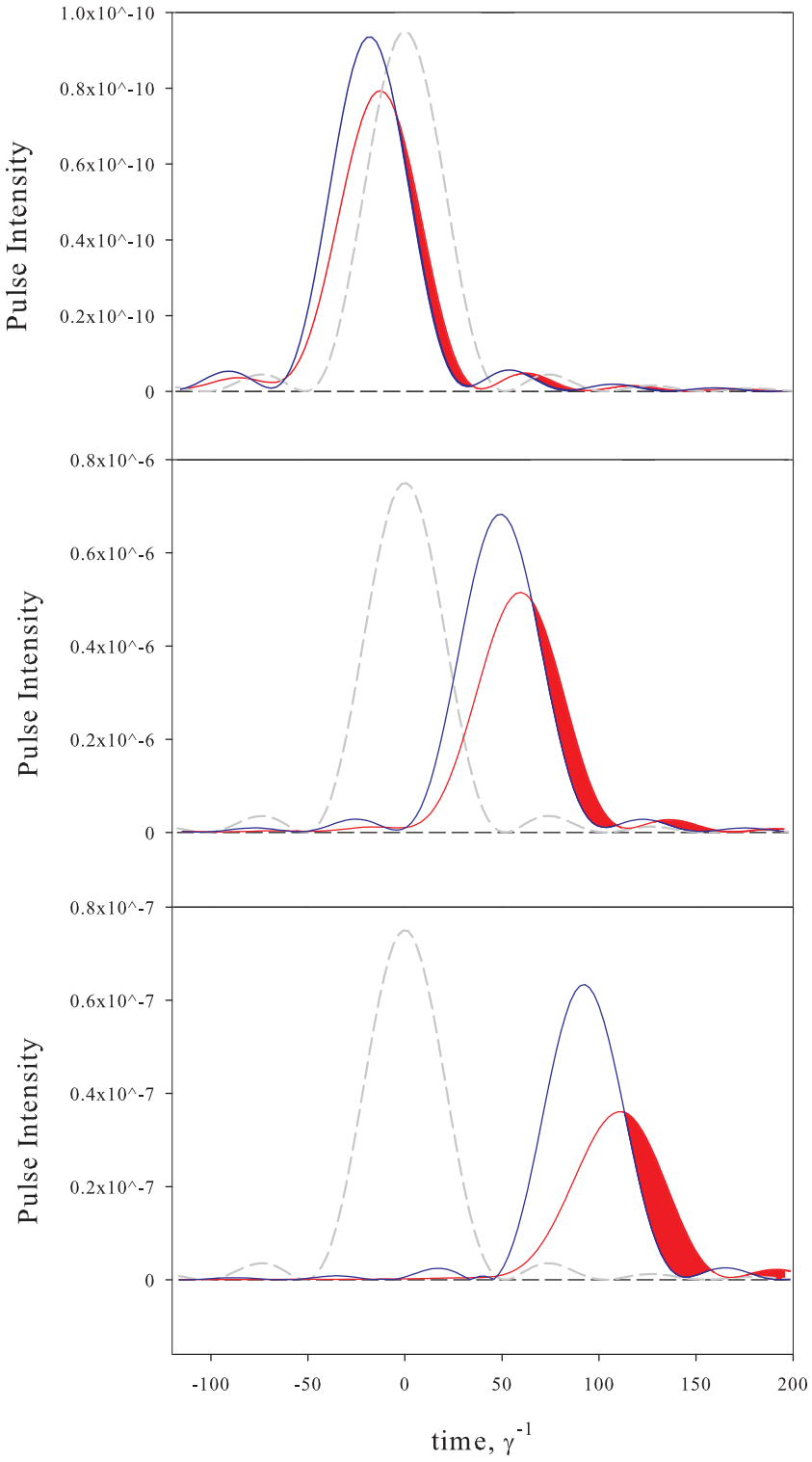

Figure 3. These graphs subsequently show the delay induced by the control field to those pulse fragments, which are freely passed forward (upper panel), and scattered in the forward direction in the 50th (central panel) and the 100th (lower panel) orders of multiple scattering. The blue curve reproduces the pulse fragment without action of the control mode and the red filled area shows the delay induced by this mode. The grey dashed curve indicates the original profile (with arbitrarily shown amplitude) of the pulse incident on the sample and the fragment intensities are scaled with respect to its original intensity.

atomic ensemble consisted of the spin-oriented atoms, which would select the Λ-type optical transitions with the highest coupling strength. However, even in the case of weak AT resonance for high scattering orders the delay effect becomes quite visible such that a significant part of the light can be stored in the spin subsystem. As was pointed out in the introduction, for diffusive propagation the light can experience several hundred scattering events before it leaves the sample.

The Monte Carlo simulations normally give a rather realistic approximation of light diffusion to an experimental

situation but it cannot demonstrate the real potential for the scheme of diffuse light storage in its optimal regime. As known from many discussions of more simple and traditional one-dimensional realizations of either EIT or Raman memory protocols, see review [21] and reference therein, the 'write-in' and 'read-out' stages of the protocol are not completely symmetric parts of the entire process. Such an asymmetry was originally pointed out in [31] for a photonic echo scheme of the quantum memory where it was shown that the retrieval of the signal pulse can be effectively made by applying the control mode in the backward direction, a point that is physically supported by time reversal arguments. Similarly, the reversion dynamics of the controllable inhomogeneous broadening plays a crucial rule for pulse retrieval in the case of the photonic echo protocol, see [23] as a clear example. In particular, for the case of a stimulated Raman process in its optimal configuration the stored signal light can be effectively mapped onto the spin coherence localized near the edge of the atomic sample where light enters the sample. This yields a very effective retrieval in the backward direction, as was confirmed by the round of calculations presented in [32] for cesium atoms. In the discussed case, we can also expect the optimal light conversion to the spin coherence near that boundary of the atomic cloud where the incident light penetrates. Then, for the best strategy in the write-in stage of the memory protocol, the optimal spectrum for the signal light should be concentrated near the steep part of the dispersion such that its further retrieval in the forward direction would be ineffective and accompanied by strong spontaneous losses. The time reversal retrieval scheme would be not so easy to organize in the three-dimensional disordered configuration, see [20], and one can use an extremely weak control mode in the read-out stage of the protocol to solve the problem and minimize spontaneous losses. In this paper, we shall discuss one specific application example where it is not necessary to retrieve the pulse in its original mode and it is only important to provide its effective storage, such that the protocol does not require the light transport throughout the whole sample. For this special situation, the above memory scheme is expected to be much more effective than its one-dimensional counterpart.

3. Quantum hologram

The proposed memory scheme is applicable and adjusted to the situation when the quantum information is originally encoded in the total number of photons in the signal light beam(s); this number is considered as a quantum variable. Such variables are insensitive to either a spatial or a temporal mode structure of the signal light pulse. Physically, this means that an unknown number of informative photons can be mapped onto the atomic subsystem via Raman-induced repopulation of the equivalent unknown number of the atoms to the signal level while light diffusely propagates through the sample. Such a situation takes place with storage of the macroscopic analogue of the Bell state; this consists of pairs of photons with either (orthogonal) horizontal (H) or vertical (V) polarizations having unknown but strongly correlated photon numbers, see [26]. In this paper,

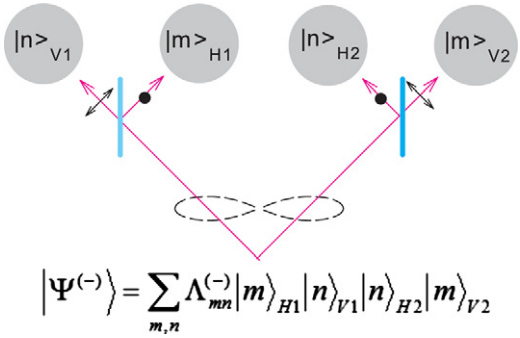

Figure 4. The quantum hologram of the macroscopically entangled state of light $|\Psi^{(-)}\rangle$, which can be prepared by a SPDC process, see [26]. The unknown photon numbers in each polarization are subsequently stored in four memory units.

we shall consider, as an example, the following entangled quantum state of light:

$$|\Psi^{(-)}\rangle = \sum_{m,n} \Lambda^{(-)}_{mn} |m\rangle_{\mathrm{H1}} |n\rangle_{\mathrm{V1}} |m\rangle_{\mathrm{V2}} |n\rangle_{\mathrm{H2}}, \tag{3}$$

where

$$\Lambda^{(-)}_{mn} = (-)^n \frac{\bar{n}^{\frac{m+n}{2}}}{[1+\bar{n}]^{\frac{m+n}{2}+1}}, \tag{4}$$

which possesses completely anti-correlated polarizations in the light beams 1 and 2, these beams propagate in different directions. The unique property of this state is that detection of a certain number of photons in any polarization (not only in H or V but also in any elliptical polarization mode) in beam 1 guarantees the detection of the same number of photons in beam 2 but always in an orthogonal polarization state. In [26], such a state was called a macroscopic analogue of a singlet-type two-particle Bell state. Its Schmidt decomposition, given by equations (3) and (4), can be found via basic expansion for the two-mode squeezed state, see [33]. The quantum state (3) can be parameterized by the average number of photons in each light beam $\bar{n}$. The unique properties of such light are fully reproducible by the above expansion and the conversion of the entangled beam states into atomic coherence can be treated as their quantum hologram. We follow here such a definition to emphasize that the atomic memory for this specific light requires storage of two spatial modes that suggests the term of quantum hologram normally used for spatially sensitive three-dimensional schemes of quantum memories, see [34, 21].

In figure 4, we illustrate how the quantum hologram of this light can be realized with the memory units, as described above. Each memory unit stores the photons of a particular polarization and frequency, which diffusely propagate through an atomic cloud and are substantially trapped on the closed transition and the stimulated Raman process is initiated by interaction with the control mode ω_c on other hyperfine sublevels ($F = 3, 2$) as is shown in the transition diagram of figure 1. The more subtle point of this process is that it creates a pure quantum state in the atomic subsystem, which is entangled among the four clouds and has an unknown but strongly correlated number of atoms repopulated onto the signal level $F_0 = 2$ in each cloud, such that their further measurement would demonstrate the presence of quantum non-locality in the matter subsystem.

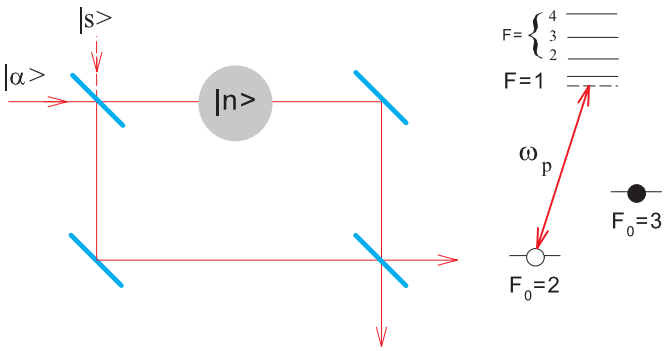

Figure 5. Schematic diagram of the Mach–Zehnder interferometer for detecting a small number of atoms stored in a particular cloud. The weak probe coherent mode $|\alpha\rangle$ of frequency ω_p is applied near the resonance of the closed $F_0 = 2 \to F = 1$ transition to avoid effects of Raman scattering. The sensitivity of the interferometer can be enhanced via sending a portion of the squeezed light $|s\rangle$ to the second input port of the interferometer, see [35].

A standard strategy for a quantum memory normally aims towards a goal of recovery of the signal pulse in its original mode. In our situation, there is no need to do that since all the quantum information is encoded into the numbers of repopulated atoms. The observation or detection of these numbers can be organized with the Mach–Zehnder interferometer, as is shown in figure 5. The interferometer can be adjusted for balanced detection of the signal expressed by the difference of the photocurrents from the output ports. Then, the measured signal associated with the small informative phase shift $\delta\phi$, induced in one arm of the interferometer, is given by

$$i_- = i_1 - i_2 \propto \bar{i}\,\delta\phi, \quad \delta\phi = \xi\, n, \tag{5}$$

where the phase shift is proportional to the number of detected atoms n and to a small factor $\xi \ll 1$, which depends on geometry (sample size, aperture of the light beam etc) and reflects the weakness of the signal. The D_2-line energy structure of an alkali-metal atom allows one to tune the probe near the resonance associated with the closed transition and to avoid any negative presence of the Raman scattering channel. In the case of ^{85}Rb, that is, the $F_0 = 2 \to F = 1$ transition. Then, the standard sensitivity of the measurement is limited by the shot-noise, Poissonian level, but it can be essentially improved via sending a portion of squeezed light to the second port of the interferometer, see [35].

Let us make the following remark concerning the above detection scheme, which in an ideal situation would perform a certain type of quantum non-demolition measurement (QND), see [36]. At first sight, the scheme seems it is specifically related to the polarization basis $|\mathrm{H}\rangle$ and $|\mathrm{V}\rangle$, which was used in expansion (3) and in the storage protocol shown in figure 4. However, an identical expansion could be rewritten in any other basis of arbitrary orthogonal elliptical polarizations and this would be described by the same expansion coefficients. In other words, the state $|\Psi^{(-)}\rangle$ is insensitive to the type of polarization beamsplitters used for the hologram creation. Then, the above QND operation with the hologram can be interpreted as postponed detection of the photons transmitted by the particular beamsplitters. With variation of the beamsplitter types, the measurement statistics could demonstrate violation of the classical probability principles. In a particular case of a rare flux consisting of the photons' pairs prepared in a 'singlet state', the measurements would show violation of the Bell inequalities. We can also point out that the hologram yields various interferometric operations and could potentially be interesting as a logic element for the further quantum information processing based on a continuous variables' scheme.

Acknowledgments

We thank Maria Chekhova and Timur Iskhakov for fruitful discussions, which initiated this work. The work was supported by RFBR (grant 10-02-00103), RFBR-CNRS (grant 12-02-91056), NSF (grant NSF-PHY-1068159) and by Federal Program 'Scientific and scientific-pedagogical personnel of innovative Russia on 2009–2013' (contract #14.740.11.0891). LVG appreciates financial support from the Charitable Foundation 'Dynasty'.

Appendix. The sample susceptibility, scattering tensor and calculation details

The susceptibility tensor responsible for elastic and mesoscopically averaged propagation of the signal mode, or of any its scattered fragments, through the atomic sample can be introduced in its major reference frame. For the excitation geometry shown in figure 1 where the control mode is linearly polarized along the Z-axis it has the following diagonal form:

$$\hat{\chi} = \begin{pmatrix} \chi_\perp & 0 & 0 \\ 0 & \chi_\perp & 0 \\ 0 & 0 & \chi_\parallel \end{pmatrix}, \tag{A.1}$$

where the $\chi_\parallel$ component determines the response of the atomic polarization on its excitation by the probe mode linearly polarized along the direction of the Z-axis and the transverse component $\chi_\perp$ gives the response of the probe for any polarization in the (X, Y)-plane. As an example, in figure A1 we show the excitation diagram of ^{85}Rb when the polarization vector of the signal mode is orthogonal to the polarization vector of the control field.

For an ensemble of motionless atomic scatterers distributed in space with density $n_0(\mathbf{r})$, the major components of the susceptibility tensor are given by

$$\chi_{\mathrm{j}}(\mathbf{r};\omega) = -n_0(\mathbf{r})\frac{1}{2F_0+1}\sum_m\sum_{n,n'} \times \frac{1}{\hbar}(\mathbf{de}_{\mathrm{j}})^*_{nm}(\mathbf{de}_{\mathrm{j}})_{n'm}\, G^{(--)}_{nn'}(\hbar\omega + E_m + \mathrm{i}0) \tag{A.2}$$

where $\mathrm{j} = X, Y(\perp);\ Z(\parallel)$ and $\left(\mathbf{de}_{\mathrm{j}}\right)_{nm}$ are the matrix elements between the ground ($|m\rangle$) and excited ($|n\rangle$ and $|n'\rangle$) states for the atomic dipole operator projected on the major axis directions. The ground state Zeeman sublevels are specified by the quantum numbers $m \equiv F_0, M_0$, where $F_0 = F_+ \equiv I+1/2$ is the total (electronic $S = 1/2$ and nuclear I) angular momentum of the upper hyperfine sublevel and M_0 is its projection. Each Zeeman sublevel has energy E_m and all of them are assumed

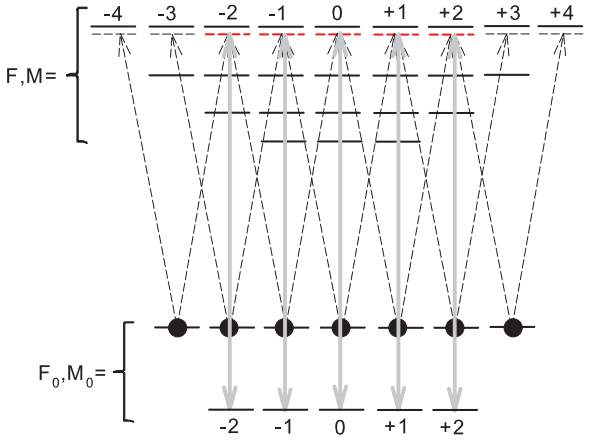

Figure A1. The scheme of excitation of ^{85}Rb, when the signal mode (dashed arrow lines) is orthogonally polarized to the control mode (gray arrow lines). The control mode is linearly polarized and the quantization axis Z is directed along its polarization, see figures 1 and 2.

to be equally populated. The quantum numbers $n \equiv F, M$ and $n' \equiv F', M'$ belong to the set of those Zeeman states of the hyperfine sublevels $F = I + 3/2, \ldots, I - 3/2$ of the excited state in the D_2 line, which are accessible by excitation for the signal mode, see the excitation diagram shown in figure A1.

The most important ingredient contributing to equation (A.2) is the retarded-type atomic Green's function of the excited state $G^{(--)}_{nn'}(E)$. For the upper exited state $|n\rangle$ with $F = F_{\max} \equiv I + 3/2$, which is not disturbed by the control mode, this function is simply defined

$$G^{(--)}_{nn'}(E) = \delta_{nn'} \frac{\hbar}{E - E_n + \mathrm{i}\hbar\gamma/2}, \tag{A.3}$$

where E_n is the energy of the state and γ is its natural relaxation rate. Green's functions for two other contributing states $|n\rangle, |n'\rangle$ form a matrix block of 2×2 (with $F = I+1/2, I-1/2$ and with same M). However, these atomic resonances are strongly affected by the interaction with the control mode such that the full set of the coupled master equations generally includes a block of 3×3 matrix components $G^{(--)}_{nn'}(E)$ (with $F = I + 1/2, I - 1/2$ and additionally $F = I - 3/2$ all with same M, see figure A1) and this block of equations is given by

$$\sum_{n''} \left[\left(E - E_n + \mathrm{i}\hbar\frac{\gamma}{2} \right) \delta_{nn''} - \frac{V_{nm'} V^*_{n''m'}}{E - \hbar\omega_c - E_{m'}} \right] G^{(--)}_{n''n'}(E) = \hbar\delta_{nn'} \tag{A.4}$$

where $V_{nm'}$ and $V_{n''m'}$ are the matrix elements of interaction with the control mode. It is important that for each particular block of states $|n\rangle, |n'\rangle$ and $|n''\rangle$, there is only one Zeeman sublevel in the ground state $|m'\rangle \equiv (F_0 = F_- = I-1/2, M_0 = M)$, which is coupled with them. The same is also valid for the populated state $|m\rangle$, if one reconsiders the problem in the basis of circular polarizations in the (X, Y)-plane, as is shown in figure A1. This basis is given by the following alternative complete set of unit vectors:

$$\mathbf{e}_0 = \mathbf{e}_Z, \quad \mathbf{e}_{\pm 1} = \mp \frac{\mathbf{e}_X \pm \mathrm{i}\mathbf{e}_Y}{\sqrt{2}}, \tag{A.5}$$

and it was used in our calculations. Thus, for each particular block of states $|n\rangle$, $|n'\rangle$ and $|n''\rangle$ there is only one pair of the Λ-coupled Zeeman sublevels $|m\rangle$ and $|m'\rangle$ in the ground state and each block of equations (A.4) is fully specified by only one state $|m\rangle$.

The susceptibility tensor in its major frame can be subsequently built via analytical solution of equations (A.4) for each m and next by substituting the result into expression (A.2). Then, the tensor's components in an arbitrary frame can be found via general rotational transformation. The 'dressing' of the atoms by the control mode creates a quasi-energy resonance structure, which is known as the AT effect, see [37, 38], and the location of the AT resonances is shown by dashed red bars in figure A1. Because of the AT effect, the susceptibility tensor becomes anisotropic and in an arbitrary (x, y, z)-reference frame can be naturally divided into linear isotropic and nonlinear anisotropic parts as follows:

$$\chi_{ij}(\omega) = \chi_0(\omega)\delta_{ij} + \chi^{(\mathrm{AT})}_{ij}(\omega), \quad i, j = (x, y, z), \tag{A.6}$$

which, in our case, consists of a dominant linear isotropic term $\chi_0(\omega)$ and a nonlinear anisotropic correction $\chi^{(\mathrm{AT})}_{ij}(\omega)$ associated with the 'dressing' of the upper state by the control mode.

Any probe wave impinging a medium and originally freely propagating in it will be scattered by atomic dipoles. The scattering process in the medium is conveniently described by the scattering tensor formalism, see [39]. This tensor is responsible for frequency- and polarization-dependent transformations of an incident electromagnetic plane wave as a result of its scattering on an isolated atom. The scattering tensor is given by

$$\begin{aligned} \hat{\alpha}^{(m''m)}_{pq}(\omega) &\equiv \alpha^{(m''m)}_{pq}(\omega) |m''\rangle\langle m| \\ &= -\sum_{n,n'} \frac{1}{\hbar} (d_p)_{m''n} (d_q)_{n'm} G^{(--)}_{nn'} \\ &\quad \times (\hbar\omega + E_m + \mathrm{i}0)\, |m''\rangle\langle m|, \end{aligned} \tag{A.7}$$

where the tensor indices defined either in a Cartesian basis $p, q = x, y, z$ or in a complex angular momentum basis $p, q = 0, \pm 1$ for the atomic dipole operators can be confined with any reference frame. The most important difference between expressions (A.2) and (A.7) is that in the scattering tensor the output transition is open for any accessible atomic state $|m''\rangle$, i.e. the entire scattering process includes all the elastic Rayleigh, elastic Raman and inelastic Raman scattering channels.

The propagation of the signal pulse or its scattered fragment in any direction can be further described by the standard approach of macroscopic Maxwell theory extended by Green's function formalism, similar to how it was done in [19, 40]. That makes the background for the Monte Carlo simulations of the entire process of light diffusion. The macroscopic Green's function is given by a fundamental solution of the wave equation describing the propagation of the electromagnetic wave through the anisotropic and scattering medium. Any secondary or multiply scattered wave is generated by the sample inhomogeneity expressed by a random fluctuation of its dielectric susceptibility and the scattering tensor describes the response of this wave on the driving field.

References

[1] Anderson P W 1958 *Phys. Rev.* **109** 1492
[2] Sheng P 1995 *Introduction to Wave Scattering, Localization, and Mesoscopic Phenomena* (San Diego, CA: Academic)
[3] Wolf P E and Maret G 1985 *Phys. Rev. Lett.* **55** 2696
[4] Albada M and Lagendijk A 1985 *Phys. Rev. Lett.* **55** 2692
[5] Labeyrie G, Thomasi F, Bernard J C, Muller C A, Miniatura C and Kaiser R 1999 *Phys. Rev. Lett.* **83** 5266
[6] Labeyrie G, Muller C A, Wiersma D S, Miniatura C and Kaiser R 2000 *J. Opt. B: Quantum Semiclass. Opt.* **2** 672
[7] Kulatunga P, Sukenik C I, Balik S, Havey M D, Kupriyanov D V and Sokolov I M 2003 *Phys. Rev.* A **68** 033816
[8] Kupriyanov D V, Sokolov I M, Larionov N V, Kulatunga P, Sukenik C I and Havey M D 2004 *Phys. Rev.* A **69** 033801
[9] Laberyrie G 2008 *Mod. Phys. Lett.* B **22** 73
[10] Kupriyanov D V, Sokolov I M, Sukenik C I and Havey M D 2006 *Laser Phys. Lett.* **3** 223
[11] Sokolov I M, Kupriyanova M D, Kupriyanov D V and Havey M D 2009 *Phys. Rev.* A **79** 053405
[12] Bienaime T, Bux S, Lucioni E, Courteille P W, Piovella N and Kaiser R 2010 *Phys. Rev. Lett.* **104** 183602
[13] Guerin W, Mercadier N, Brivio D and Kaiser R 2009 *Opt. Express* **17** 14
[14] Kaiser R 2012 private communication
[15] Letokhov V S 1968 *Sov. Phys.—JETP* **26** 835
[16] Billy J, Josse V, Zuo Z, Bernard A, Hambrecht B, Lugan P, Clement D, Sanches-Palencia L, Bouyer P and Aspect A 2008 *Nature* **453** 891
[17] Roati G, D'Errico C, Fallani L, Fattori M, Fort C, Zaccanti M, Modugno G, Modugno M and Inguscio M 2008 *Nature* **453** 895
[18] Kondov S S, McGehee W R, Zirbel J J and DeMarco B 2011 *Science* **334** 66
[19] Datsyuk V M, Kupriyanov D V, Sokolov I M and Havey M D 2006 *Phys. Rev.* A **74** 043812
[20] Gerasimov L V, Sokolov I M, Olave R G and Havey M D 2011 *J. Opt. Soc. Am.* B **28** 1459
[21] Polzik E, Sørensen A and Hammerer K 2010 *Rev. Mod. Phys.* **82** 1041
[22] Simon C *et al* 2010 *Eur. Phys. J.* D **58** 1–22
[23] Hosseini M, Sparkes B M, Campbell G, Lam P K and Buchler B C 2011 *Nature Commun.* **2** 174
[24] Scherman M, Mishina O S, Lombardi P, Laurat J and Giacobino E 2011 arXiv:1106.0988v2
Mishina O S, Scherman M, Lombardi P, Ortalo J, Felinto D, Sheremet A S, Bramati A, Kupriyanov D V, Laurat J and Giacobino E 2011 *Phys. Rev.* A **83** 033838
[25] Froufe-Pérez L S, Guerin W, Carminati R and Kaiser R 2009 *Phys. Rev. Lett.* **102** 173903
Guerin W, Mercadier N, Michaud F, Brivio D, Froufe-Pérez L S, Carminati R, Eremeev V, Goetschy A, Skipetrov S I and Kaiser R 2010 *J. Opt.* **12** 024002
[26] Iskhakov T S, Chekhova M V, Rytikov G O and Leuchs G 2011 *Phys. Rev. Lett.* **106** 113602
[27] Matsko A B, Novikova I, Welsh G R, Budker D, Kimball D F and Rochester S M 2002 *Phys. Rev.* A **66** 043815
[28] Mikhailov E E and Novikova I 2008 *Opt. Lett.* **33** 1213
[29] Horrom T, Balik S, Lezama A, Havey M D and Mikhailov E E 2011 *Phys. Rev.* A **83** 053850
[30] Barreiro S, Valente V, Failache H and Lezama A 2011 *Phys. Rev.* A **84** 033851
[31] Moiseev S A and Kroll S 2001 *Phys. Rev. Lett.* **87** 173601
Moiseev S A and Noskov N I 2004 *Laser Phys. Lett.* **1** 303
[32] Sheremet A S, Gerasimov L V, Sokolov I M, Kupriyanov D V, Mishina O S, Giacobino E and Laurat J 2010 *Phys. Rev.* A **82** 033838
[33] Braunstein S L and van Loock P 2005 *Rev. Mod. Phys.* **77** 513
[34] Vasiliev D V, Sokolov I V and Polzik E S 2008 *Phys. Rev.* A **77** 020302
[35] Xiao M, Wu L A and Kimble H J 1987 *Phys. Rev. Lett.* **59** 278
[36] Mandel E and Wolf L 1995 *Optical Coherence and Quantum Optics* (Cambridge: Cambridge University Press)
[37] Autler S H and Townes C H 1955 *Phys. Rev.* **100** 703
[38] Letokhov V S and Chebotaev V P 1977 *Nonlinear Laser Spectroscopy* (Berlin: Springer)
[39] Beresteskii V B, Lifshits E M and Pitaevskii L P 1981 *Course of Theoretical Physics: Quantum Electrodynamics* (Oxford: Pergamon)
[40] Datsyuk V M, Sokolov I M, Kupriyanov D V and Havey M D 2008 *Phys. Rev.* A **77** 033823
Sokolov I M, Kupriyanov D V, Olave R G and Havey M D 2010 *J. Mod. Opt.* **57** 1833